Acta Oceanol. Sin., 2025, Vol. 44, No. 9, P. 81–94
https://doi.org/10.1007/s13131-025-2511-3

Geochemical characteristics and petrogenesis of the basaltic pyroclastic rocks from the Xisha Islands, northwestern South China Sea

Yu Zhang[1], Yaqi Yuan[1], Kefu Yu[1, 2*]

[1] Guangxi Laboratory on the Study of Coral Reefs in the South China Sea and School of Marine Sciences, Guangxi University, Nanning 530004, China
[2] Southern Marine Science and Engineering Guangdong Laboratory (Guangzhou), Guangzhou 511458, China

Received 6 January 2025; accepted 25 April 2025
© Chinese Society for Oceanography and Springer-Verlag GmbH Germany, part of Springer Nature 2025

Abstract
As one of the micro-blocks dispersed in the South China Sea (SCS), the Xisha Islands are covered by thick Cenozoic sedimentary layers, making it challenging to obtain magmatic rocks. Well CK-2 is a kilometer-scale scientific drilling project on the Xisha Islands in the northwestern SCS. It penetrates the thick reef limestone and reaches basaltic pyroclastic rocks. This study presents the whole-rock and olivine compositions of the basaltic volcaniclastic rocks from Well CK-2. These rocks exhibited ocean island basalt signatures characterized by the enrichment of light rare earth elements and high-field-strength elements. Compared with partial melting products derived from mantle peridotite, whole-rock compositions showed elevated Fe/Mn and Zn/Fe mass ratios. Additionally, olivines were characterized by a lower Ca content, higher Ni content, elevated Fe/Mn mass ratios, and moderate Mn/Zn mass ratios compared to those crystallized from peridotitic melts. The compositions of both the whole-rock and olivine phenocrysts indicate the presence of pyroxenite in the mantle source, which likely formed through the reaction of recycled oceanic crust with the surrounding mantle peridotite. Using the olivine-liquid Mg-Fe exchange thermometer, this study derived mantle potential temperatures (T_p) ranging from 1 502℃ to 1 756℃, which is consistent with those of plume-related ocean island basalts. Furthermore, the basaltic volcaniclastic rocks exhibit low H_2O contents (0.01%–1.47%), which were significantly lower than those found in the primary magmas of Large Igneous Provinces. These results suggest that the basaltic volcaniclastic rocks on the Xisha Islands originated from a volatile-poor mantle plume source.

Key words South China Sea, Xisha Islands, basaltic pyroclastic rocks, olivine

Citation Zhang Yu, Yuan Yaqi, Yu Kefu. 2025. Geochemical characteristics and petrogenesis of the basaltic pyroclastic rocks from the Xisha Islands, northwestern South China Sea. Acta Oceanologica Sinica, 44(9): 81–94, doi: 10.1007/s13131-025-2511-3

1 Introduction

The South China Sea (SCS) is one of the largest marginal basins in the western Pacific that is located at the junction of the Pacific, Eurasian, and Indo-Australian Plates (Li et al., 2015; Yang and Fang, 2015; Yu et al., 2018; Zhang et al., 2018a, 2018b; Yu and Liu, 2020). Although the SCS basin is relatively small and its oceanic crust is very young, it has undergone a nearly complete Wilson cycle, from continental breakup to seafloor spreading to subduction (Li et al., 2014; Yang and Fang, 2015; Yang et al., 2019). Thus, the SCS serves as a natural laboratory for studying various lithospheric evolutionary processes, including continental margin breakup, ocean basin expansion, and subduction termination, and has attracted widespread attention from researchers worldwide (Li et al., 2014, 2015; Yu et al., 2018). The SCS can be divided into three main parts: northern, southern, and oceanic basins. The northern margin of the SCS lies between the South China Block and the ocean-continent transition zone of the SCS. In the past, the northern margin of the SCS was classified as a discrete, non-volcanic,

Foundation item: The National Natural Science Foundation of China under contract No. 42030502; the Guangxi Scientific Projects under contract Nos. AD17129063, AA17204074, and 2025GXNSFAA069324; the NSFC project under contract No. 42166003.
*Corresponding author, E-mail: kefuyu@scsio.ac.cn

passive continental margin (Clift et al., 2002). However, with the progression of research, it has been regarded as representing an intermediate mode of rifting, bearing characteristics that are closely aligned with a magma-poor margin (Gao et al., 2015). Unlike volcanic margins, which are characterized by extensive magmatic activity, Cenozoic volcanic rocks along the northern margin of the SCS are relatively limited in distribution. However, post-spreading magmatism is widespread throughout the SCS and surrounding areas (Xu et al., 2012).

The northern continental margin of the SCS has long been influenced by subduction of the Mesozoic Paleo-Pacific Plate and Cenozoic rifting processes (Suo et al., 2019; Li et al., 2020; Sun et al., 2021; Zhang et al., 2021a; Yang et al., 2023). Since the Late Cenozoic, the region has been influenced by a complex interplay of geological processes, including seafloor spreading, subduction along the Manila Trench, formation of the Taiwan Orogeny, uplift of the Tibetan Plateau, and extrusion of the Indosinian Block. These geological processes led to frequent and intense magmatic activity along passive continental margins during the Late Cenozoic (Zhang et al., 2014).

The Xisha Islands are overlain by thick Cenozoic sediments at the northern continental margin of the SCS, making it challenging to access magmatic rock samples through drilling. Consequently, studies on mantle-derived magmatism and tectonic evolution in the Xisha region remain scarce. Whether the Cenozoic magmatic activity in the Xisha region is related to the Hainan mantle plume remain unclear, which directly affects our understanding of critical scientific issues, such as the extensional processes of the northern SCS margin and the regional tectono-magmatic evolution. In this study, we present the mineral chemistry and whole-rock geochemistry of basaltic pyroclastic rocks from the basement of Well CK-2 to reveal the lithology of the mantle source and nature of the primary magma, which aids in our understanding of the genesis of Cenozoic basalts in the SCS and their geodynamic background.

2 Geological setting and sample description

The SCS is bounded by the East Vietnam fault to the west and the Manila Trench the east (Fig. 1). The deep-water basin of the SCS can be divided into three sub-basins: southwest, east, and northwest (Li et al., 2014, 2015; Liao et al., 2022; Zhang et al., 2024). Constrained by mapping magnetic anomalies and International Ocean Discovery Program Expedition (IODP) 349 drilling results, the onset of seafloor spreading near the northern continental margin of the SCS was dated to approximately 33 Ma. Subsequently, around 23.6 Ma, the ridge jumped southward and the seafloor extended into the southwest sub-basin. Seafloor spreading ceased at approximately 15 Ma in the eastern sub-basin and approximately 16 Ma in the southwestern sub-basin (Li et al., 2014). After the cessation of seafloor spreading, post-spreading magmatism occurred widely in the SCS and the surrounding areas (Wang et al., 2012; Xu et al., 2012; Yan et al., 2018, 2019; Yu et al., 2018; Qian et al., 2021, 2022).

There are several micro-blocks dispersed in the SCS, including Xisha, Nansha, Zhongsha, and Reed-northeastern Palawan blocks (Yan et al., 2008, 2014, 2015; Liu et al., 2011; Li et al., 2013; Zhang et al., 2020b, 2024). During the Paleo-Tethyes period, these micro-blocks were regarded as a single block, which was named the "Qiongdongnan block" (Liu et al., 2006; Yan et al., 2008). Since the Early Cenozoic, the regional stress field shifted from compression to extension, causing these micro-blocks to rift and drift away from the South China block (Clift et al., 2008; Yan et al., 2019 and references therein).

The Xisha micro-block is situated in the northwestern part of the northern continental slope of the SCS, bounded by the Xisha Trough in the north, the Qiongdongnan Basin in the northwest, and the Dongsha Trough in the east (Fig. 1). Composed of thinned continental crust, its basement is believed to have been affected by multiple phases of magmatism (Huang et al., 2011; Guo et al., 2016; Li et al., 2019; Zhang et al., 2024 and reference therein). With the subsidence of the Xisha micro-block and global sea-level fluctuations, coral reefs in the Xisha region began to develop since the Early Miocene (Shao et al., 2017; Fan et al., 2020). During the Middle Miocene, reefs flourished and expanded laterally, reaching their maximum extent (Wang et al., 2018). However, they began to contract during the Late Miocene and shrank further into isolated carbonate platforms during the Pliocene and Pleistocene (Wu et al., 2014).

Well CK2 was drilled in the Xisha micro-block of the northwestern SCS (Fig. 1). The well was drilled through thick reefal limestone (0–878.21 m) and reached the underlying basement (878.21–928.75 m) (Fig. 2). The basement of Well CK-2 consisted of basaltic pyroclastic rocks. The basaltic pyroclastic rocks contain minor amounts of marine bioclastic fossils, occasionally accompanied by reef limestone breccias (Fig. 3). They were predominantly gray-green, dark green, and yellow-brown in color. They underwent extensive alteration (chloritization, serpentinization and carbonation) and exhibited well-developed vesicular and amygdaloidal textures. The amygdalae were predominantly elliptical and circular, with a few irregularly shaped amygdales. The filling minerals mainly consisted of calcite, opal, chalcedony, and zeolite. The crystalline clastic minerals were primarily composed of clinopyroxene with minor amounts of plagioclase and olivine. The crystal clastics were mostly sub-angular to angular in shape, indicating that the basaltic pyroclastic rocks were formed in situ or near the site of volcanic activity. For a more detailed petrographic analysis, please refer to Zhang et al. (2018c, 2020b, 2024). The chemical characteristics of the clinopyroxene indicated that the parent magma belonged to a silica-undersaturated alkaline series, formed in an intraplate tectonic setting (Zhang et al., 2018c). The zircon U-Pb geochronology of the basaltic

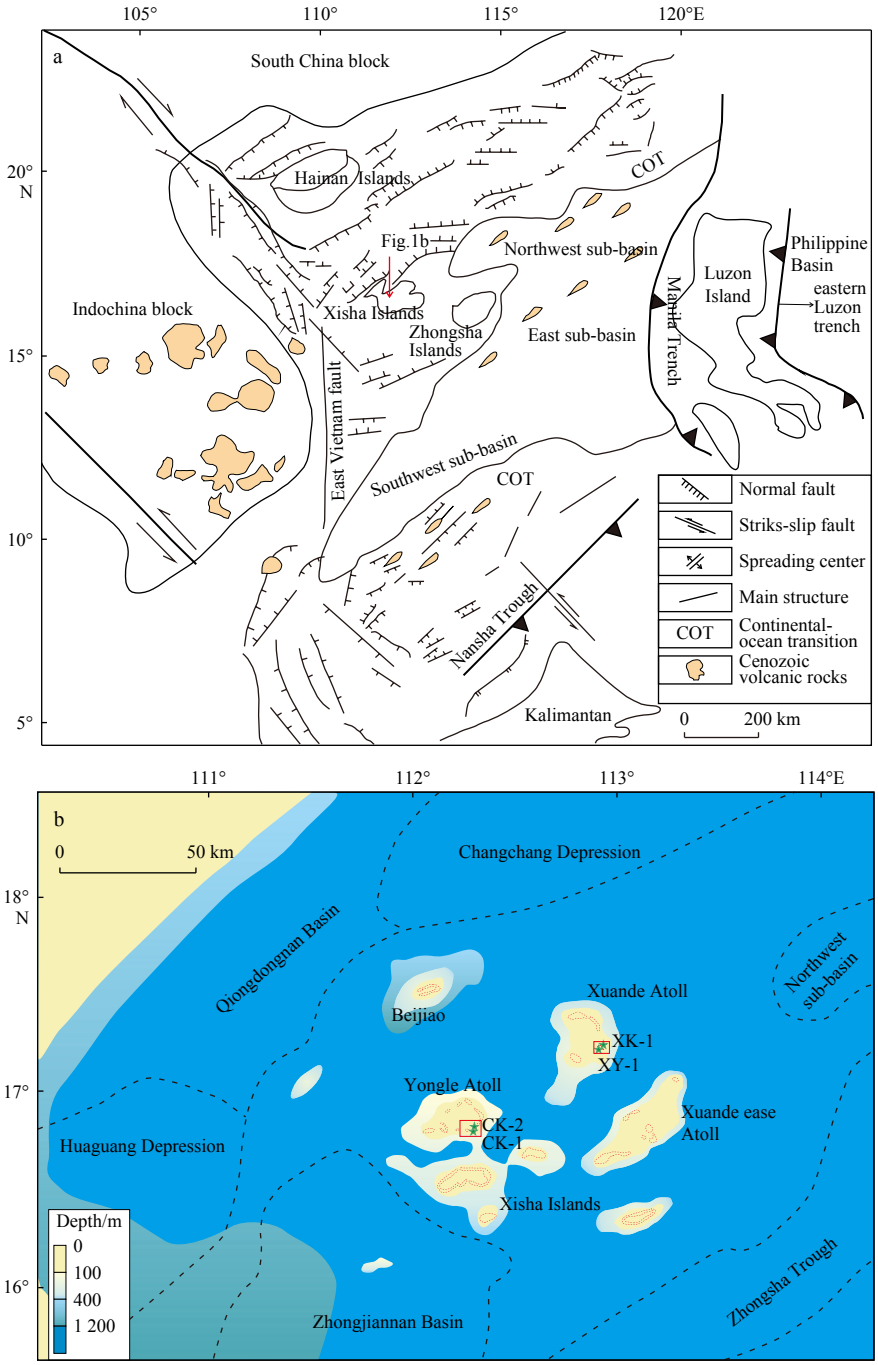

Fig. 1. Geological sketch of the SCS and its adjacent areas (a); location of Well CK-2 (b) (Wang et al., 2018; Zhang et al., 2024). The depth is below sea level and in meters.

pyroclastic rocks indicated that the Xisha micro-block likely developed on a uniform Late Jurassic metamorphic crystalline basement intruded by Cretaceous granitic magmatism (Zhang et al., 2024).

3 Analytical methods

In this study, whole-rock geochemical analyses of basaltic pyroclastic rocks were conducted using the LA-ICP-MS method. The sample selection adhered to the following two criteria: (1) microscopic observation ensured that the samples did not undergo significant alteration and (2) preference was given to fine-grained samples with evenly distributed mineral grains (Yang, 2015). Whole-rock LA-ICP-MS analyses were performed at the State Key Laboratory of Ore Deposit Geochemistry, Institute of Geochemistry, Chinese Academy of Sciences, using an Agilent 7 900 ICP-MS equipped with a GeoLasPro 193 nm ArF excimer laser. Helium was applied as a carrier gas which was mixed with Argon via a T-connector before entering the ICP-MS. The standard ablation cell was optimized with resin mold to get a small volume and to improve the washout efficiency. Analysis was run with 44 μm pit size, 10 Hz pulse frequency and 4−5 J/cm^2 fluence. El-

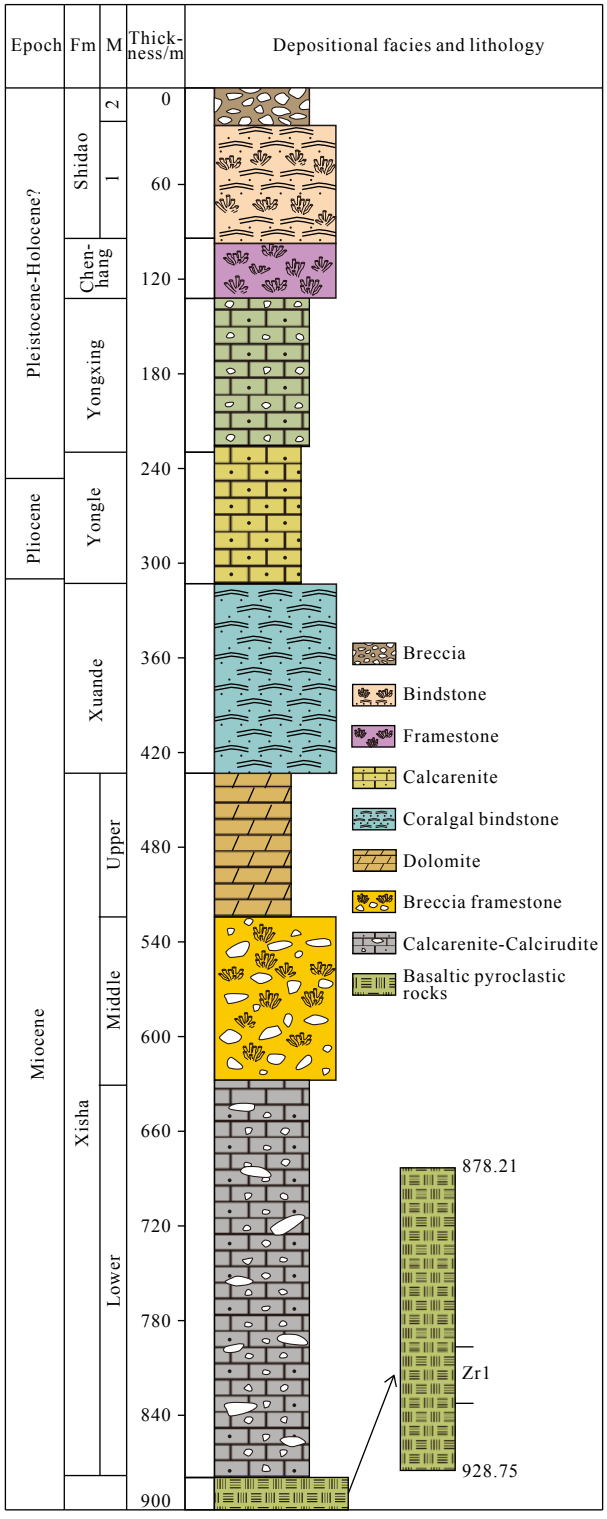

Fig. 2. Stratigraphy of Well CK-2, Xisha Islands (Zhang et al., 2020a). Fm: Formation; M: member.

ement contents were calibrated against multiple-reference materials (BHVO-2G, BCR-2G, and BIR-1G) without using an internal standard (Liu et al., 2008b). Off-line selection and integration of the background and analyte signals, time-drift correction, and quantitative calibration were performed using ICPMSDataCal (Liu et al., 2010).

In-situ trace element analyses of olivine were carried out using LA-ICP-MS at the Wuhan SampleSolution Analytical Technology Co., Ltd., Wuhan China. Detailed instrument parameters and analytical procedures are same as described by Zong et al. (2017).

4 Analytical results

4.1 *Whole-rock major and trace element compositions*

The whole-rock major and trace elements are listed in Table S1. The mass fraction of the pyroclastic rockschemical composition is as follows: 40.56%–48.89% for SiO_2; 12.79%–17.46% for Al_2O_3; 13.86%–20.63% for MgO; 11.45%–16.42% for ^{T}FeO; and 0.88%–4.77% for TiO_2. The Mg# values ranged from 66 to 75. The chondrite-normalized rare-earth element (REE) patterns showed that the pyroclastic rocks were enriched in light rare earth elements (LREEs) and had flat heavy rare earth element (HREE) patterns similar to those of the SCS and intraplate ocean island basalts (OIB) (Fig. 4) (Sun and McDonough, 1989; Yan et al., 2008). In the primitive mantle-normalized trace-element spider diagram (Fig. 5), the pyroclastic rocks were characterized by enrichment in high-field-strength elements (HFSEs), consistent with the features of OIB.

4.2 *Mineral chemistry*

Twenty olivine grains were analyzed for their chemical compositions. The results are summarized in Table S2. The analyzed olivines exhibited a narrow range of Fo contents (81–84). The major elemental compositions of the olivine from the basaltic pyroclastic rocks were as follows: SiO_2, 37.36%–39.23%; MgO, 43.28%–45.08%; NiO, 0.15%–0.24%; MnO, 0.21%–0.25%; CaO, 0.16%–0.25%. The high CaO content suggests that the analyzed olivines were phenocrysts formed during magma fractional crystallization (Thompson and Gibson, 2000; Foley et al., 2013).

5 Discussion

5.1 *Crustal contamination and fractional crystallization*

The composition of the basaltic magma is influenced by crustal contamination as it ascends through the crust to the surface. Therefore, it is necessary to evaluate the impact of crustal contamination on geochemical composition before interpreting the petrogenesis of basaltic pyroclastic rocks (Rudnick and Gao, 2003; Dai et al., 2018; Zhang et al., 2020a). Previous studies suggest that crustal contamination can be identified using whole-rock isotopes and trace-elements (Rudnick and Gao, 2003; Salters and Stracke, 2004). The basaltic pyroclastic rocks exhibited a relatively variable Nb/U mass ratio (23.29–89.22, with an average of 46.46) and Ce/Pb mass ratio (1.63–36.49, with an average of 13.04), which were substantially higher than those of the continental crust (Nb/U = 6.15 and Ce/Pb = 3.91; Rudnick and Gao, 2003; Salters and

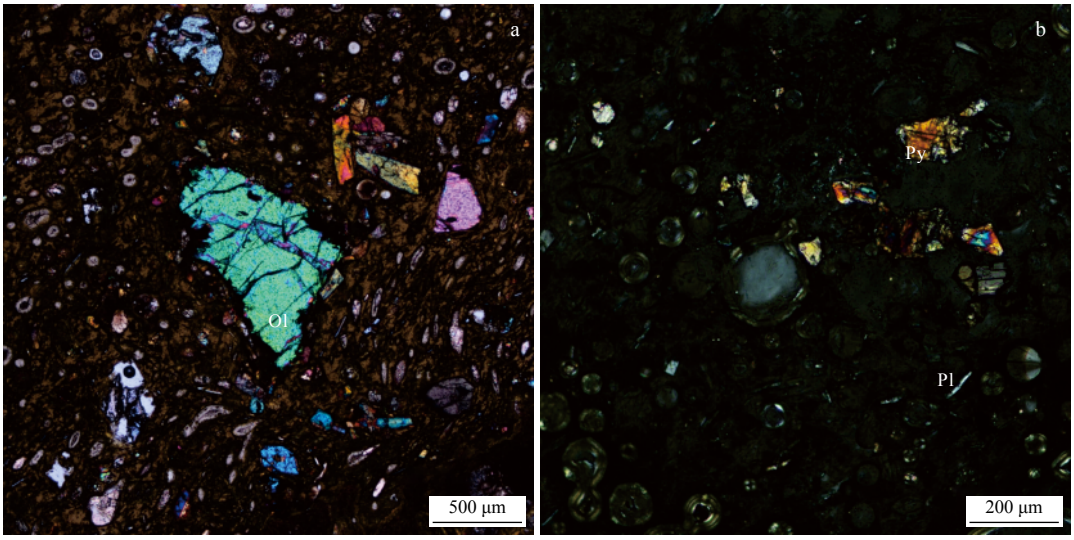

Fig. 3. Representative photomicrographs of the basaltic pyroclastic. Py: Pyroxene; Pl: Plagioclase; Ol: Olivine.

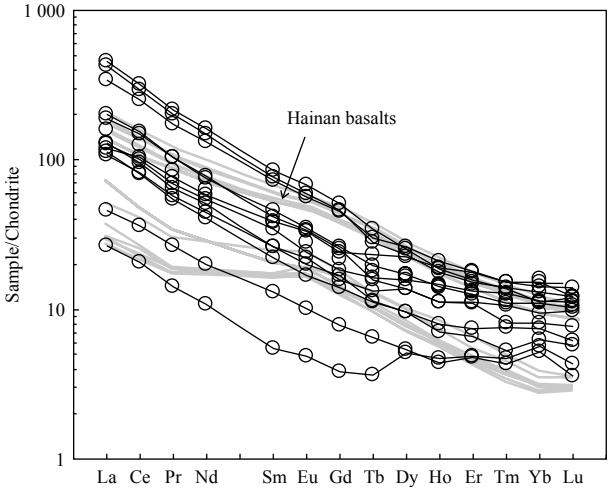

Fig. 4. Chondrite-normalized rare earth element patterns for the basaltic pyroclastic rocks from Well CK-2, Xisha Islands, SCS. The values for chondrite normalization are from Sun and McDonough (1989). Cenozoic basalt in Hainan Island is from literature (Liu et al., 2015; Gu et al., 2019).

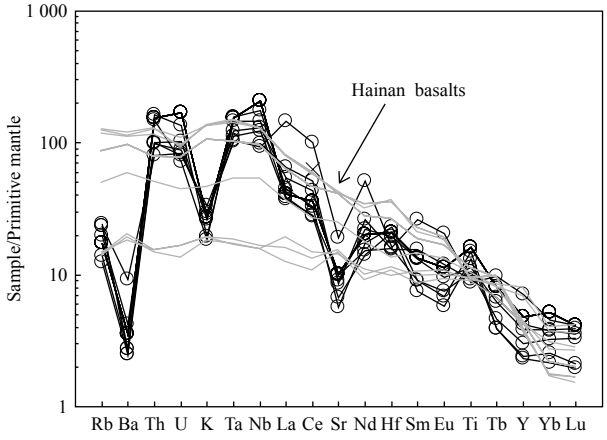

Fig. 5. Primitive mantle-normalized trace element diagrams for the basaltic pyroclastic rocks from Well CK-2, Xisha Islands, SCS. The values for primitive mantle normalization are from Sun and McDonough (1989). Cenozoic basalt in Hainan Island is from literature (Liu et al., 2015; Gu et al., 2019).

Stracke, 2004), suggesting limited crustal contamination. Furthermore, the primitive mantle-normalized trace element pattern lacked strong negative Nb or Ta anomalies (Fig. 5), implying that continental crustal contamination was negligible (Zou et al., 2003; Yang and Fang, 2015; An et al., 2017; Zhang et al., 2020a). In conclusion, the trace element characteristics suggest that crustal contamination of basaltic pyroclastic rocks was negligible, supporting the inference that these rocks were likely derived from a mantle source.

The basaltic pyroclastic rocks were characterized by low contents of Ni (131–247 μg/g), Co (16–77 μg/g), and Cr (23–73 μg/g) (Table S1). These results are inconsistent with the geochemical characteristics of primitive magma (Irving and Frey, 1978; Wilkinson and Le Maitre, 1987; An et al., 2017; Zhang et al., 2020a), implying that these basaltic pyroclastic rocks experienced a certain degree of fractional crystallization of olivine and clinopyroxene. In the primitive mantle-normalized trace-element spider diagram, the samples showed negative Eu and Sr anomalies (Fig. 5), indicating that the magmas that formed these basaltic pyroclastic rocks underwent plagioclase fractionation.

5.2 *Lithology of mantle source*

Identifying the lithology of mantle sources is essential for estimating the composition of the primary magma, assessing the mantle potential temperature, and understanding mantle heterogeneity. Traditionally, peridotite has been considered the primary mantle lithology in the source region of alkali basalts (Herzberg and O'Hara, 2002; Putirka, 2005; Rhodes et al., 2012). However, partial melting experiments have demonstrated that alkaline

basalts can also be generated through the partial melting of olivine-poor mantle lithologies, including carbonated peridotite, pyroxenite, and hornblendite (Hirschmann and Stolper, 1996; Hirschmann et al., 2003; Kogiso et al., 2003; Pertermann and Hirschmann, 2003a; Dasgupta et al., 2006, 2007; Kogiso and Hirschmann, 2006; Pilet et al., 2008; Sorbadere et al., 2013; Lambart et al., 2016).

Previous studies have suggested that carbonated peridotite and pyroxenite contribute to the mantle source of Late Cenozoic basalts in the SCS and its surrounding areas (Wang et al., 2012; Liu et al., 2015; An et al., 2017; Li et al., 2017; Zhang et al., 2017; Yan et al., 2018; Yang et al., 2020; Cao et al., 2022a, 2022b). Magmas generated through the partial melting of carbonated mantle peridotite exhibited significant negative Ti, Zr, and Hf anomalies (Zeng et al., 2010). However, the basaltic pyroclastic rocks exhibit positive Ti and Hf anomalies (Fig. 5), ruling out carbonatized mantle peridotite as the mantle source.

Experimental studies have demonstrated that the Fe/Mn mass ratio in basaltic melts serves as a reliable indicator of the mantle source lithology and can effectively distinguish between pyroxenite and peridotite mantle sources (Liu et al., 2008a; Wang et al., 2012). Pyroxenite-derived melts typically exhibit higher Fe/Mn mass ratios than those derived from peridotite (Liu et al., 2008a; Herzberg, 2011). Basaltic pyroclastic rocks are characterized by high Fe/Mn mass ratios, with an average of 86, which is significantly higher than the ratios observed in mid-ocean ridge basalt (MORB) and typical peridotite-derived melts (Wang et al., 2012). This elevated Fe/Mn mass ratio suggests the presence of a certain amount of pyroxenite in the mantle source of the basaltic pyroclastic rocks. Le Roux et al. (2010) demonstrated that high Zn/Fe mass ratios indicate a non-peridotite source. The basaltic pyroclastic rocks exhibited high Zn/Fe mass ratios (8.5–13.8, with an average of 10.7), which were substantially higher than the average values of the upper mantle (Le Roux et al., 2010). This further supported the presence of pyroxenite in the source rocks (Le Roux et al., 2010).

Olivine typically crystallizes first from mantle-derived melts, making it a key indicator for identifying the source lithology. In the basaltic pyroclastic rocks, the Fo of olivine exhibited no significant correlation with Ca content but shows a marked negative correlation with Mn content (Figs 6a and b). These systematic compositional relationships indicate that clinopyroxene fractionation has a limited influence on the olivine composition, suggesting that the observed olivine characteristics primarily reflect source-related processes. Previous studies suggest that the involvement of pyroxenite or eclogite in a mantle source can be identified by the presence of olivine phenocrysts with low content of Ca, high content of Ni, and high Fe/Mn mass ratios (Sobolev et al., 2005, 2007; Herzberg, 2011; Foley et al., 2013). The olivine phenocrysts from the basaltic pyroclastic rocks exhibited low Ca and high Ni contents, similar to the compositions of olivines in basalts from the SCS and its surrounding areas, which were derived from a pyroxenite source (Figs 6a and c) (Wang et al., 2012; Liu et al., 2015; An et al., 2017; Hoang et al., 2018; Zhang et al., 2018b; Yang et al., 2023)

Mn, Zn, and Fe have similar olivine–melt partition coefficients during the melting of mantle peridotite under specific whole-rock compositions, oxygen fugacity, pressure, and temperature conditions (Le Roux et al., 2010; Foley et al., 2013; Howarth and Harris, 2017). The proportions of these elements do not change significantly during partial melting or fractional crystallization but rather represent the characteristics of the source region (Sobolev et al., 2007; Foley et al., 2013; Herzberg et al., 2016). The Fe/Mn mass ratios of crystallized olivine from peridotite-derived melts generally ranged from 60 to 70 (Herzberg, 2011). The whole-rock high Fe/Mn ratios of the basaltic pyroclastic rocks were reflected in the Fe/Mn ratios of their olivine phenocrysts. As shown in the Fo vs. Fe/Mn diagram (Fig. 6d), most olivines from the basaltic pyroclastic rocks displayed high Fe/Mn mass ratios, indicating the presence of a pyroxenite mantle source. Howarth and Harris (2017) proposed that olivine crystallized from peridotite melts has high Mn/Zn values (>15), whereas olivine crystallized from pyroxenite melts has low Mn/Zn values (<13). The Mn/Zn values of olivine in the basaltic pyroclastic rocks range from 12 to 15, indicating a mixed pyroxenite-peridotite source. In summary, the compositions of both whole-rock (e.g., Fe/Mn and Zn/Fe mass ratios) and olivine phenocrysts (e.g., Ca and Ni contents and Fe/Mn and Zn/Fe mass ratios) suggest that the mantle source of basaltic pyroclastic rocks is a mixture of peridotite and pyroxenite.

Several hypotheses have been proposed to explain the genesis of pyroxenite, including (1) cumulative pyroxenite (Zhang and Xu, 2012), (2) metamorphosed oceanic crust (Herzberg, 2011; Lambart et al., 2013) and (3) reactions between recycled continental/oceanic crust and the surrounding mantle peridotite (Sobolev et al., 2005; Mallik and Dasgupta, 2012; Foley et al., 2013; Liu et al., 2015; Zhang et al., 2021b). Cumulative pyroxenite is characterized by low Ni content and cannot crystallize high-Ni olivine (Lee et al., 2006); therefore, the first hypothesis can be excluded. Additionally, most basaltic pyroclastic rocks have a higher MgO content than the melting products of silica-excess pyroxenite or bimineralic eclogite (MgO < 8.0%; Pertermann and Hirschmann, 2003b); the second hypothesis is not applicable for explaining the origin of the pyroxenite components in the mantle source of these rocks. Therefore, we argue that the third hypothesis is the most plausible mechanism for the genesis of pyroxenite in the source region of basaltic pyroclastic rocks.

The basaltic pyroclastic rocks exhibited positive Nb and Ta anomalies in the primitive mantle-normalized spidergrams (Fig. 5), suggesting that continental crust components were not present in the mantle source. Li is typically enriched in the crust and sediments (up to 70 μg/g) compared with the lithospheric mantle and mantle-de-

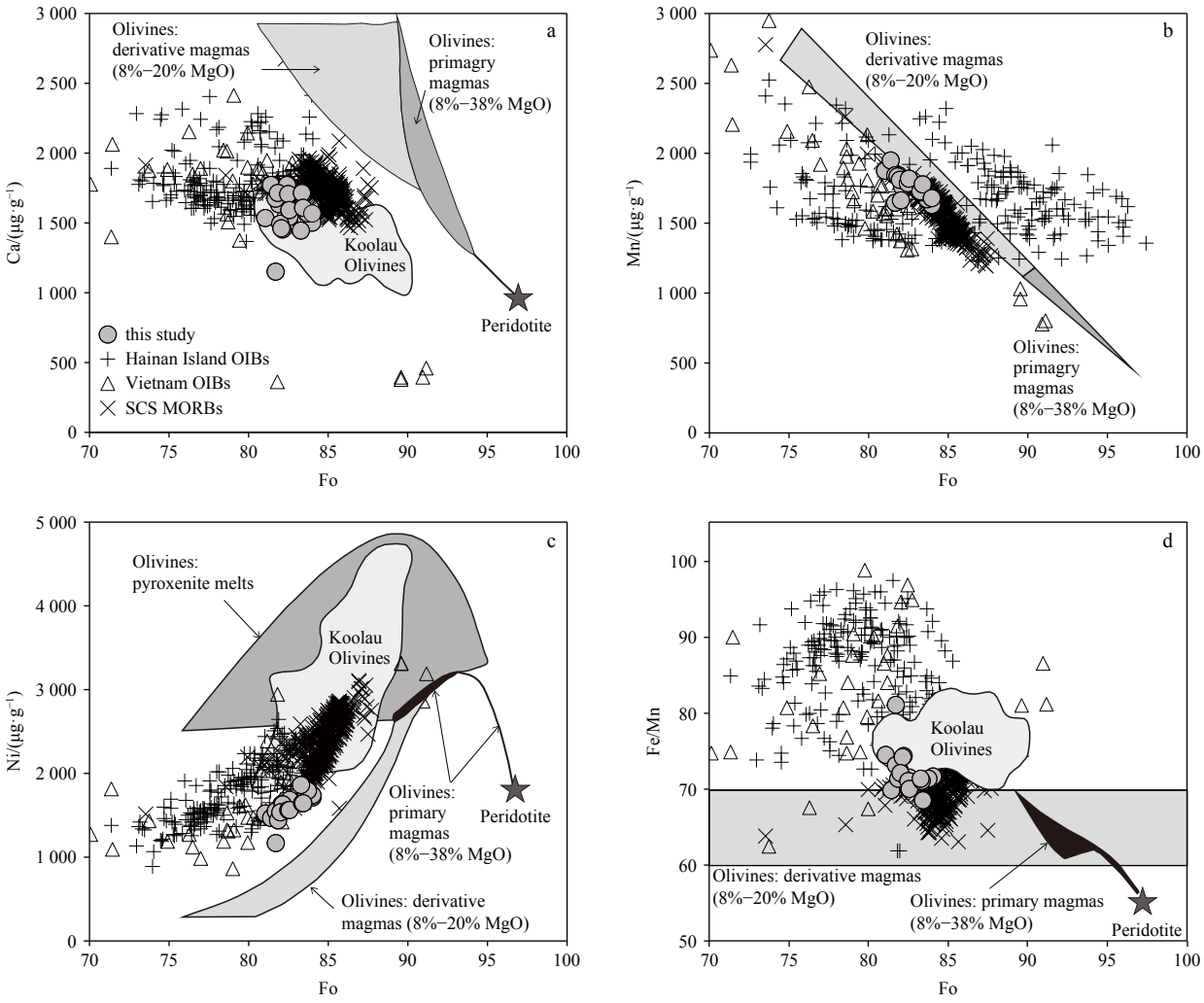

Fig. 6. Composition of olivine phenocrysts in basaltic pyroclastic rocks from Well CK-2 compared to calculated olivines from partial melts of a fertile peridotite and a stage 2 pyroxenite, after Herzberg (2011). Also shown are Koolau olivines (Sobolev et al., 2007). Data for the Hainan Island are from Gu et al. (2019); data for the Vietnam are from Hoang et al. (2018); data for SCS are from Zhang et al. (2018b).

rived melts (Foley et al., 2013). Based on the low Li content of olivine from Hawaii basalts, Ammannati et al. (2016) suggested that recycled subducted oceanic crust was involved in the production of the Hawaii basalts. The olivines from the basaltic pyroclastic rocks had low Li contents (mostly <5 μg/g), indicating that continental crust components were not present in the mantle source (Foley et al., 2013). Thus, we suggest that the recycled oceanic crust may have reacted with ambient mantle peridotite to form a relatively silica-rich mantle pyroxenite.

5.3 *Mantle potential temperature*

Potential temperature (T_p) refers to the hypothetical temperature of the mantle as it rises to Earth's surface without decompression or melting (Putirka, 2005). This serves as a critical parameter for characterizing the thermal state of the upper mantle (McKenzie and Bickle, 1988; Putirka, 2005, 2008; Campbell, 2007; Wang et al., 2012; Lee et al., 2009). It is widely recognized that magmas exhibiting OIB characteristics are not exclusively derived from mantle plumes (Xu et al., 2012). Mantle plumes are commonly linked to thermal anomalies characterized by elevated T_p values. Moreover, it is generally accepted that the generation of mafic magma associated with mantle plumes requires higher ambient T_p than that required for the formation of MORB (Herzberg and Asimow, 2008). To constrain mantle plumes, the concept of excess temperature (T_{ex}) has been proposed to identify thermal anomalies in the mantle ($T_{ex}=T_p^{hotspot}-T_p^{MORB}$). OIBs generated by mantle plumes typically exhibit elevated T_{ex}, which range between 100℃ and 300℃ (Kreutzmann et al., 2004; Putirka, 2005). Consequently, T_p can serve as a diagnostic parameter for identifying the presence of mantle plumes (Kreutzmann et al., 2004; Putirka, 2005).

The olivine-liquid Mg-Fe exchange thermometer was independent of the specific lithology of the mantle source (Putirka, 2005; Yu and Liu, 2020). In this study, we used an Fe-Mg exchange geothermometer to calculate the T_p of basaltic pyroclastic rocks. Using this method, the esti-

mated T_p for the basaltic pyroclastic rocks ranged from 1 502℃ to 1 756℃, with an average of 1 645℃. The T_p of Iceland basalt ranged from 1 480℃ to 1 520℃, and the T_p of Hawaii OIB was approximately 1 530℃ (Putirka, 2005). The estimated T_p of the basaltic pyroclastic rocks aligned closely with that of the plume-related OIBs (Iceland and Hawaii basalts), indicating an abnormally high mantle potential temperature in the study area. As discussed earlier, basaltic pyroclastic rocks exhibit OIB-like geochemical characteristics (Fig. 4). The combination of these OIB-type geochemical features and the evidence of high-temperature anomalies strongly supports the involvement of a mantle plume in their genesis.

Previous studies have proposed that the head of the Hainan mantle plume likely impinges on the base of the lithosphere at approximately 30 Ma (Wang et al., 2013). Yu et al. (2018) suggested that the SCS MORB which could have recorded plume-ridge interaction perhaps appeared since about 23.8 Ma. The initial-spreading MORB (Site U1500) of the SCS yielded a normal T_p (about 1 380℃) and was derived from a peridotite-dominated mantle source, suggesting that the opening of the SCS was not influenced by a mantle plume (Yu and Liu, 2020). In contrast, the late-spreading MORB (Site U1431E) yielded relatively high T_p (about 1 442℃) and originated from a pyroxenite-enriched mantle source (Zhang et al., 2018a, 2018b; Yang et al., 2019, 2023), indicating that the mantle plume impacted the final stages of SCS spreading. The uneven distribution of stagnant slab materials in the mantle transition zone is believed to have split and bifurcated the Cenozoic Hainan mantle plume into separate upwellings (Yang et al., 2023). Stronger portions of these stagnant slabs likely impeded the ascent of the mantle plume and hindere its upward migration. This bifurcation likely occurred as the mantle plume encountered stagnant slabs within the mantle transition zone, providing a plausible explanation for the uneven distribution of magmatic activity and discrepancies between the predicted magmatic distribution and topographic changes in classical mantle plume models (Yang et al., 2023).

5.4 *Water content of the magmas*

The formation of Large Igneous Provinces (LIP) involves various physical and chemical factors, including anomalously high mantle temperatures, the presence of fusible components in the mantle source, substantial decompression, and water enrichment (Sobolev et al., 2011; Liu et al., 2017). LIP are widely regarded as closely associated with mantle plume activity. Specifically, thermochemical mantle plumes originating from deep mantle are considered to account for the deep-sourced materials and the elevated thermal energy necessary for the extensive melting observed in LIP.

Water content of the mantle is important for studying magmatic processes in the deep mantle. Elevated water content increases the melting depth, leading to an increase in the volume of magma formed by melting. Recently, studies on the water content of major LIPs have been conducted worldwide (Xia et al., 2016; Liu et al., 2017, 2022; Ivanov et al., 2018; Gu et al., 2019; Lang et al., 2020). The primary magma water content of the picrites from the Emeishan LIP was 3.44%, corresponding to a mantle source water content of more than 6 000 μg/g. The formation of the Emeishan LIP was closely related to a high-temperature mantle plume enriched in water and fusible components (Liu et al., 2017).

The water content of the mantle plays a critical role in understanding magmatic processes occurring in the deep mantle. Elevated water content enhances the melting depth, which in turn increases the volume of magma produced during melting. Recent studies have investigated the water content of the mantle sources in major LIP (Xia et al., 2016a; Liu et al., 2017, 2022; Ivanov et al., 2018; Gu et al., 2019; Lang et al., 2020). For instance, the primary magma water content of the picrites from the Emeishan LIP exhibited a water content of 3.44%, corresponding to a mantle source water content exceeding 6 000 μg/g (Liu et al., 2017). The formation of the Emeishan LIP was closely related to a high-temperature mantle plume enriched in both water and fusible components (Liu et al., 2017).

In this study, the water content of the basaltic pyroclastic rocks was estimated using a Ca-in-olivine geohygrometer (Gavrilenko et al., 2016). This geohygrometer is based on experimental observations that demonstrate the influence of meltwater content on the partition coefficient of CaO between olivine and silicate melts ($D_{CaO}^{ol/liq}$). The geohygrometer calculated the meltwater content as a function of the MgO content and $D_{CaO}^{ol/liq}$ with an estimated uncertainty of 1.4%–1.8% H_2O (Gavrilenko et al., 2016). Using this method, we determined the H_2O contents of the primary magma in basaltic pyroclastic rocks to be 0.01%–1.47% (with an average of 0.66%), which is comparable to the water content of OIB (0.3%–2%, Métrich et al., 2014). However, these values were significantly lower than those of the mantle sources for many LIPs, such as the Emeishan LIP (3.44%, Liu et al., 2017) and the Tarim LIP (4.8%, Xia et al., 2016a) (Fig. 7).

5.5 *Implications*

Accumulating geophysical and geochemical evidence increasingly supports the existence of a Hainan mantle plume (Zou and Fan, 2010; Wang et al., 2013; Huang, 2014; Wei and Chen, 2016; Xia et al., 2016b; An et al., 2017; Fan et al., 2017; Yan et al., 2018, 2019; Yu et al., 2018; Zhang et al., 2018b, 2020a). A mushroom-shaped low-velocity seismic anomaly extending into the lower mantle was identified, suggesting the presence of a lower mantle root associated with the Hainan plume beneath southern China (Huang et al., 2015; Wei and Chen, 2016; Xia et al., 2016b; Fan et al., 2017). Several geophysical studies have further suggested that the Hainan mantle plume is one of the 12 plumes originating from the core-mantle boundary (Huang et al., 2015). The Cenozoic in-

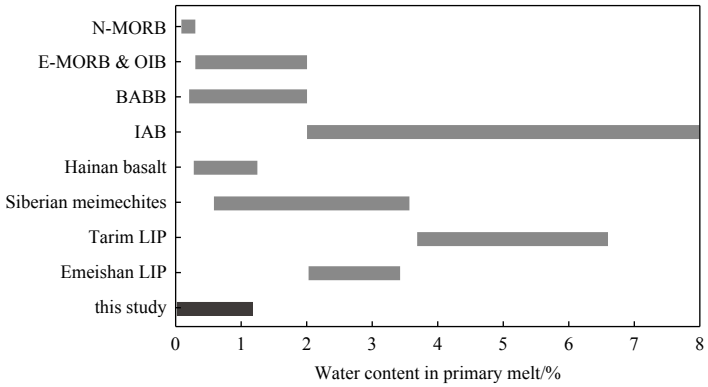

Fig. 7. Comparison of water contents in the primary melts of the basaltic pyroclastic rocks with those in other primary melts from different geological settings. The water contents of the Hainan basalts are from Gu et al. (2019) and those of other melts from Liu et al. (2017) and references therein. N-MORB: normal mid-ocean ridge basalt; E-MORB: enriched mid-ocean ridge basalt; OIB: oceanic island basalt; BABB: back-arc basin basalt; IAB: island arc basalt

traplate basalts of Southeast Asia are primarily distributed across the Leizhou Peninsula, Hainan Island, Indochina block, and SCS.

Gravity and magnetic anomaly data indicate that Cenozoic magmatism was widely distributed in the Xisha area (Zhang et al., 2016; Feng et al., 2017). Zhang et al. (2016) identified flat-topped and conical-topped seamounts in the Xisha area based on the geophysical data. Chenhang Island potentially represent one of the flat-topped seamounts (Zhang et al., 2024). The stratigraphic contact relationship and seismic reflection characteristics revealed three distinct phases of magmatism in the Xisha area: Paleocene and Eocene, early Oligocene to mid-Miocene, and mid-Miocene to recent (Zhang et al., 2016). In this study, the trace element patterns of the basaltic pyroclastic rocks exhibited typical OIB-like characteristics (Fig. 4). Additionally, the high T_p values further support the hypothesis that the mantle beneath the Xisha Islands was significantly influenced by the Hainan mantle plume. The northwestern SCS has experienced multiple phases of rifting since the Late Cretaceous, characterized by the extensive development of NE-NEE trending faults, which provide favorable pathways for magma upwelling. Furthermore, mantle plume material underwent lateral expansion at lithospheric depths, affecting the entire northern SCS from west to east (Xia et al., 2025). This process likely drives the widespread magmatic activity observed in the Xisha area. However, unlike classical mantle columns with large heads and thin tails that form large igneous provinces and age-progressive seamount chains, the Hainan mantle column did not exhibit these features.

6 Conclusions

This study presents the whole-rock and olivine chemical compositions of basaltic pyroclastic rocks from Well CK-2, SCS, and reaches to the following conclusions:

The compositions of both whole-rock and olivine phenocrysts indicate that the mantle source of the basaltic pyroclastic rocks was derived from a mixed source comprising peridotite and pyroxenite. The pyroxenite likely formed through the reaction of recycled oceanic crust with the surrounding mantle peridotite.

The calculated T_p values ranged from 1 502℃ to 1 756℃, which were comparable to those of plume-related OIB.

The basaltic pyroclastic rocks exhibited low H_2O contents (0.01%–1.47%), significantly lower than those observed in the primary magmas of LIPs.

References

Ammannati E, Jacob D E, Avanzinelli R, et al. 2016. Low Ni olivine in silica-undersaturated ultrapotassic igneous rocks as evidence for carbonate metasomatism in the mantle. Earth and Planetary Science Letters, 444: 64–74, doi: 10.1016/j.epsl.2016.03.039

An A R, Choi S H, Yu Y, et al. 2017. Petrogenesis of late Cenozoic basaltic rocks from southern Vietnam. Lithos, 272–273: 192–204, doi: 10.1016/j.lithos.2016.12.008

Campbell I H. 2007. Testing the plume theory. Chemical Geology, 241(3–4): 153–176, doi: 10.1016/j.chemgeo.2007.01.024

Cao Guangyue, Tong Ying, Li Xiang, et al. 2022a. Insights from olivine chemistry into crustal magmatic processes and the mantle source lithology of basalts from Hainan Island, China. Lithos, 430–431: 106852, doi: 10.1016/j.lithos.2022.106852

Cao Chuqi, Xiong Fahui, Yang Shengbiao, et al. 2022b. Geochemical characteristics and petrogenesis of Cenozoic basalt from the northern continental margin of the South China Sea. Acta Geologica Sinica (in Chinese), 96(8): 2683–2704

Cheng Zhiguo, Zhang Zhaochong, Wang Zhenchao, et al. 2020. Petrogenesis of transitional large igneous province: insights from bimodal volcanic suite in the Tarim large igneous province. Journal of Geophysical Research: Solid Earth, 125(5): e2019JB018382, doi: 10.1029/2019JB018382

Clift P, Lee G H, Anh Duc N, et al. 2008. Seismic reflection ev-

idence for a Dangerous Grounds miniplate: no extrusion origin for the South China Sea. Tectonics, 27(3): TC3008, doi: 10.1029/2007TC002216

Clift P, Lin Jian, Barckhausen U. 2002. Evidence of low flexural rigidity and low viscosity lower continental crust during continental break-up in the South China Sea. Marine and Petroleum Geology, 19(8): 951–970, doi: 10.1016/S0264-8172(02)00108-3

Dai Liqun, Zheng Fei, Zhao Zifu, et al. 2018. Geochemical insights into the lithology of mantle sources for Cenozoic alkali basalts in West Qinling, China. Lithos, 302–303: 86–98, doi: 10.1016/j.lithos.2017.12.013

Dasgupta R, Hirschmann M M, Smith N D. 2007. Partial melting experiments of peridotite + CO_2 at 3 GPa and genesis of alkalic ocean island basalts. Journal of Petrology, 48(11): 2093–2124, doi: 10.1093/petrology/egm053

Dasgupta R, Hirschmann M M, Stalker K. 2006. Immiscible transition from carbonate-rich to silicate-rich melts in the 3 GPa melting interval of eclogite + CO_2 and genesis of silica-undersaturated ocean island lavas. Journal of Petrology, 47(4): 647–671, doi: 10.1093/petrology/egi088

Fan Chaoyan, Xia Shaohong, Zhao Fang, et al. 2017. New insights into the magmatism in the northern margin of the South China Sea: spatial features and volume of intraplate seamounts. Geochemistry, Geophysics, Geosystems, 18(6): 2216–2239, doi: 10.1002/2016GC006792

Fan Tianlai, Yu Kefu, Zhao Jianxin, et al. 2020. Strontium isotope stratigraphy and paleomagnetic age constraints on the evolution history of coral reef islands, northern South China Sea. GSA Bulletin, 132(3–4): 803–816, doi: 10.1130/B35088.1

Feng Yingci, Zhan Wenhuan, Sun Jie, et al. 2017. The formation mechanism and characteristics of volcanoes in the Xisha waters since Pliocene. Journal of Tropical Oceanography (in Chinese), 36(3): 73–79

Foley S F, Prelevic D, Rehfeldt T, et al. 2013. Minor and trace elements in olivines as probes into early igneous and mantle melting processes. Earth and Planetary Science Letters, 363: 181–191, doi: 10.1016/j.epsl.2012.11.025

Gao Jinwei, Wu Shiguo, McIntosh K, et al. 2015. The continent–ocean transition at the mid-northern margin of the South China Sea. Tectonophysics, 654: 1–19, doi: 10.1016/j.tecto.2015.03.003

Gavrilenko M, Herzberg C, Vidito C, et al. 2016. A calcium-in-olivine geohygrometer and its application to subduction zone magmatism. Journal of Petrology, 57(9): 1811–1832, doi: 10.1093/petrology/egw062

Gu Xiaoyan, Wang Piaoyi, Kuritani T, et al. 2019. Low water content in the mantle source of the Hainan plume as a factor inhibiting the formation of a large igneous province. Earth and Planetary Science Letters, 515: 221–230, doi: 10.1016/j.epsl.2019.03.034

Guo Xiaoran, Zhao Minghui, Huang Haibo, et al. 2016. Crustal structure of Xisha block and its tectonic attributes. Chinese Journal of Geophysics (in Chinese), 59(4): 1414–1425

Herzberg C. 2011. Identification of source lithology in the Hawaiian and Canary Islands: implications for origins. Journal of Petrology, 52(1): 113–146, doi: 10.1093/petrology/egq075

Herzberg C, Asimow P D. 2008. Petrology of some oceanic island basalts: PRIMELT2. XLS software for primary magma calculation. Geochemistry, Geophysics, Geosystems, 9(9): Q09001, doi: 10.1029/2008GC002057

Herzberg C, O'Hara M J. 2002. Plume-associated ultramafic magmas of Phanerozoic age. Journal of Petrology, 43(10): 1857–1883, doi: 10.1093/petrology/43.10.1857

Herzberg C, Vidito C, Starkey N A. 2016. Nickel–cobalt contents of olivine record origins of mantle peridotite and related rocks. American Mineralogist, 101(9): 1952–1966, doi: 10.2138/am-2016-5538

Hirschmann M M, Kogiso T, Baker M B, et al. 2003. Alkalic magmas generated by partial melting of garnet pyroxenite. Geology, 31(6): 481–484, doi: 10.1130/0091-7613(2003)031<0481:AMGBPM>2.0.CO;2

Hirschmann M M, Stolper E M. 1996. A possible role for garnet pyroxenite in the origin of the "garnet signature" in MORB. Contributions to Mineralogy and Petrology, 124(2): 185–208, doi: 10.1007/s004100050184

Hoang T H A, Choi S H, Yu Y, et al. 2018. Geochemical constraints on the spatial distribution of recycled oceanic crust in the mantle source of late Cenozoic basalts, Vietnam. Lithos, 296: 382395, doi: 10.1016/j.lithos.2017.11.020

Holloway N H. 1982. North Palawan block, Philippine-its relation to Asian mainland and role in evolution of South China Sea. AAPG Bulletin, 66(9): 1355–1383, doi: 10.1306/03B5A7A5-16D1-11D7-8645000102C1865D

Howarth G H, Harris C. 2017. Discriminating between pyroxenite and peridotite sources for continental flood basalts (CFB) in southern Africa using olivine chemistry. Earth and Planetary Science Letters, 475: 143–151, doi: 10.1016/j.epsl.2017.07.043

Hu Zhaochu, Zhang Wen, Liu Yongsheng, et al. 2015. "Wave" signal-smoothing and mercury-removing device for laser ablation quadrupole and multiple collector ICPMS analysis: application to lead isotope analysis. Analytical Chemistry, 87(2): 1152–1157, doi: 10.1021/ac503749k

Huang Jinli. 2014. P- and S-wave tomography of the Hainan and surrounding regions: insight into the Hainan plume. Tectonophysics, 633: 176–192, doi: 10.1016/j.tecto.2014.07.007

Huang Haibo, Qiu Xuelin, Xu Yi, et al. 2011. Crustal structure beneath the Xisha Islands of the South China Sea simulated by the teleseismic receiver function method. Chinese Journal of Geophysics (in Chinese), 54(11): 2788–2798, doi: 10.3969/j.issn.0001-5733.2011.11.009

Huang Zhouchuan, Zhao Dapeng, Wang Liangshu. 2015. *P* wave tomography and anisotropy beneath Southeast Asia: insight into mantle dynamics. Journal of Geophysical Research: Solid Earth, 120(7): 5154–5174, doi: 10.1002/2015JB012098

Irving A J, Frey F A. 1978. Distribution of trace elements between garnet megacrysts and host volcanic liquids of kimberlitic to rhyolitic composition. Geochimica et Cosmochimica Acta, 42(6): 771–787, doi: 10.1016/0016-7037(78)90092-3

Ivanov A V, Mukasa S B, Kamenetsky V S, et al. 2018. Volatile

concentrations in olivine-hosted melt inclusions from meimechite and melanephelinite lavas of the Siberian Traps Large Igneous Province: evidence for flux-related high-Ti, high-Mg magmatism. Chemical Geology, 483: 442–462, doi: 10.1016/j.chemgeo.2018.03.011

Kogiso T, Hirschmann M M. 2006. Partial melting experiments of bimineralic eclogite and the role of recycled mafic oceanic crust in the genesis of ocean island basalts. Earth and Planetary Science Letters, 249(3–4): 188–199, doi: 10.1016/j.epsl.2006.07.016

Kogiso T, Hirschmann M M, Frost D J. 2003. High-pressure partial melting of garnet pyroxenite: possible mafic lithologies in the source of ocean island basalts. Earth and Planetary Science Letters, 216(4): 603–617, doi: 10.1016/S0012-821X(03)00538-7

Kreutzmann A, Schmeling H, Junge A, et al. 2004. Temperature and melting of a ridge-centred plume with application to Iceland. Part II: predictions for electromagnetic and seismic observables. Geophysical Journal International, 159(3): 1097–1111, doi: 10.1111/j.1365-246X.2004.02397.x

Kushiro I. 1996. Partial melting of a fertile mantle peridotite at high pressures: an experimental study using aggregates of diamond. In: Basu A, Hart S, eds. Earth Processes: Reading the Isotopic Code. Washington: American Geophysical Union, 109–122, doi: 10.1029/GM095p0109

Lambart S, Baker M B, Stolper E M. 2016. The role of pyroxenite in basalt genesis: melt-PX, a melting parameterization for mantle pyroxenites between 0.9 and 5 GPa. Journal of Geophysical Research: Solid Earth, 121(8): 5708–5735, doi: 10.1002/2015JB012762

Lambart S, Laporte D, Schiano P. 2013. Markers of the pyroxenite contribution in the major-element compositions of oceanic basalts: review of the experimental constraints. Lithos, 160–161: 14–36, doi: 10.1016/j.lithos.2012.11.018

Lang Mingde, Cheng Zhiguo, Zhang Zhaochong, et al. 2020. Hisingerite in trachydacite from Tarim: implications for voluminous felsic rocks in transitional large igneous province. Journal of Earth Science, 31(5): 875–883, doi: 10.1007/s12583-020-1330-x

Le Bas M J, Le Maitre R W, Streckeisen A, et al. 1986. A chemical classification of volcanic rocks based on the total alkali-silica diagram. Journal of Petrology, 27(3): 745–750, doi: 10.1093/PETROLOGY/27.3.745

Le Roux V, Lee C T A, Turner S J. 2010. Zn/Fe systematics in mafic and ultramafic systems: implications for detecting major element heterogeneities in the earth's mantle. Geochimica et Cosmochimica Acta, 74(9): 2779–2796, doi: 10.1016/j.gca.2010.02.004

Lee C T A, Cheng Xin, Horodyskyj U. 2006. The development and refinement of continental arcs by primary basaltic magmatism, garnet pyroxenite accumulation, basaltic recharge and delamination: insights from the Sierra Nevada, California. Contributions to Mineralogy and Petrology, 151(2): 222–242, doi: 10.1007/s00410-005-0056-1

Lee C T A, Luffi P, Plank T, et al. 2009. Constraints on the depths and temperatures of basaltic magma generation on Earth and other terrestrial planets using new thermobarometers for mafic magmas. Earth and Planetary Science Letters, 279(1–2): 20–33, doi: 10.1016/j.epsl.2008.12.020

Li Chunfeng, Li Jiabiao, Ding Weiwei, et al. 2015. Seismic stratigraphy of the central South China Sea basin and implications for neotectonics. Journal of Geophysical Research: Solid Earth, 120(3): 1377–1399, doi: 10.1002/2014JB011686

Li Chunfeng, Lin Jian, Kulhanek D K. 2014. South China Sea tectonics: opening of the South China Sea and its implications for Southeast Asian tectonics, climates, and deep mantle processes since the late Mesozoic. International Ocean Discovery Program Scientific Prospectus, 349: 1–111

Li Fucheng, Sun Zhen, Yang Hongfeng, et al. 2020. Continental interior and edge breakup at convergent margins induced by subduction direction reversal: a numerical modeling study applied to the South China sea margin. Tectonics, 39(11): e2020TC006409, doi: 10.1029/2020TC006409

Li Naisheng, Yan Quanshu, Chen Zhihua, et al. 2013. Geochemistry and petrogenesis of Quaternary volcanism from the islets in the eastern Beibu Gulf: evidence for Hainan plume. Acta Oceanologica Sinica, 32(12): 40–49, doi: 10.1007/s13131-013-0386-1

Li Shuguang, Yang Wei, Ke Shan, et al. 2017. Deep carbon cycles constrained by a large-scale mantle Mg isotope anomaly in eastern China. National Science Review, 4(1): 111–120, doi: 10.1093/nsr/nww070

Li Shiying, Yu Kefu, Zhang Yu, et al. 2019. Mineral chemistry of clinopyroxene in pyroclastic rocks of the Xisha Islands and their geological significance. Haiyang Xuebao (in Chinese), 41(7): 65–76

Liao Renqiang, Zhu Hongli, Li Congying, et al. 2022. Geochemistry of mantle source during the initial expansion and its implications for the opening of the South China Sea. Marine Geology, 447: 106798, doi: 10.1016/j.margeo.2022.106798

Liu Yongsheng, Gao Shan, Hu Zhaochu, et al. 2010. Continental and oceanic crust recycling-induced melt-peridotite interactions in the Trans-North China Orogen: U-Pb dating, Hf isotopes and trace elements in zircons from mantle xenoliths. Journal of Petrology, 51(1–2): 537–571, doi: 10.1093/petrology/egp082

Liu Yongsheng, Gao Shan, Kelemen P B, et al. 2008a. Recycled crust controls contrasting source compositions of Mesozoic and Cenozoic basalts in the North China Craton. Geochimica et Cosmochimica Acta, 72(9): 2349–2376, doi: 10.1016/j.gca.2008.02.018

Liu Yongsheng, Hu Zhaochu, Gao Shan, et al. 2008b. *In situ* analysis of major and trace elements of anhydrous minerals by LA-ICP-MS without applying an internal standard. Chemical Geology, 257(1–2): 34–43, doi: 10.1016/j.chemgeo.2008.08.004

Liu Jianqiang, Ren Zhongyuan, Nichols A R L, et al. 2015. Petrogenesis of Late Cenozoic basalts from North Hainan Island: constraints from melt inclusions and their host olivines. Geochimica et Cosmochimica Acta, 152: 89–

121, doi: 10.1016/j.gca.2014.12.023

Liu Jia, Xia Qunke, Kuritani T, et al. 2017. Mantle hydration and the role of water in the generation of large igneous provinces. Nature Communications, 8(1): 1824, doi: 10.1038/s41467-017-01940-3

Liu Jia, Xia Qunke, Sun Hao, et al. 2022. Compositional variation of picrites in the Emeishan large igneous province modulated by water in the mantle plume. Journal of Geophysical Research: Solid Earth, 127(1): e2021JB023584, doi: 10.1029/2021JB023584

Liu Hailing, Yan Pin, Liu Yingchun, et al. 2006. Existence of Qiongnan suture zone on the north margin of South China Sea. Chinese Science Bulletin, 51(S2): 107–120, doi: 10.1007/s11434-006-9107-x

Liu Hailing, Yan Pin, Zhang Boyou, et al. 2004. Pre-Cenozoic basements of the South China Sea and eastern Tethyan realm. Marine Geology & Quaternary Geology (in Chinese), 24(1): 15–28

Liu Hailing, Zheng Hongbo, Wang Yanlin, et al. 2011. Basement of the South China Sea area: tracing the Tethyan realm. Acta Geologica Sinica-English Edition, 85(3): 637–655, doi: 10.1111/j.1755-6724.2011.00457.x

Mallik A, Dasgupta R. 2012. Reaction between MORB-eclogite derived melts and fertile peridotite and generation of ocean island basalts. Earth and Planetary Science Letters, 329–330: 97–108, doi: 10.1016/j.epsl.2012.02.007

McKenzie D, Bickle M J. 1988. The volume and composition of melt generated by extension of the lithosphere. Journal of Petrology, 29(3): 625–679, doi: 10.1093/petrology/29.3.625

Métrich N, Zanon V, Créon L, et al. 2014. Is the 'Azores hotspot' a wetspot? Insights from the geochemistry of fluid and melt inclusions in olivine of Pico basalts. Journal of Petrology, 55: 377–393, doi: 10.1093/petrology/egt071

Pertermann M, Hirschmann M M. 2003a. Partial melting experiments on a MORB-like pyroxenite between 2 and 3 GPa: constraints on the presence of pyroxenite in basalt source regions from solidus location and melting rate. Journal of Geophysical Research: Solid Earth, 108(B2): 2125, doi: 10.1029/2000JB000118

Pertermann M, Hirschmann M M. 2003b. Anhydrous partial melting experiments on MORB-like eclogite: phase relations, phase compositions and mineral-melt partitioning of major elements at 2–3 GPa. Journal of Petrology, 44(12): 2173–2201, doi: 10.1093/petrology/egg074

Pilet S, Baker M B, Stolper E M. 2008. Metasomatized lithosphere and the origin of alkaline lavas. Science, 320(5878): 916–919, doi: 10.1126/science.1156563

Putirka K D. 2005. Mantle potential temperatures at Hawaii, Iceland, and the mid-ocean ridge system, as inferred from olivine phenocrysts: evidence for thermally driven mantle plumes. Geochemistry, Geophysics, Geosystem, 6(5): Q05L08, doi: 10.1029/2005GC000915

Putirka K D. 2008. Thermometers and barometers for volcanic systems. Reviews in Mineralogy and Geochemistry, 69(1): 61–120, doi: 10.2138/rmg.2008.69.3

Qian Shengping, Gazel E, Nichols A R L, et al. 2021. The origin of Late Cenozoic magmatism in the South China Sea and Southeast Asia. Geochemistry, Geophysics, Geosystems, 22(8): e2021GC009686, doi: 10.1029/2021GC009686

Qian Shengping, Salters V, McCoy-West A J, et al. 2022. Highly heterogeneous mantle caused by recycling of oceanic lithosphere from the mantle transition zone. Earth and Planetary Science Letters, 593: 117679, doi: 10.1016/j.epsl.2022.117679

Rhodes J M, Huang Shichun, Frey F A, et al. 2012. Compositional diversity of Mauna Kea shield lavas recovered by the Hawaii Scientific Drilling Project: inferences on source lithology, magma supply, and the role of multiple volcanoes. Geochemistry, Geophysics, Geosystems, 13(3): Q03014, doi: 10.1029/2011GC003812

Rudnick R L, Gao Shan. 2003. Composition of the continental crust. Treatise on Geochemistry, 3: 1–64, doi: 10.1016/B0-08-043751-6/03016-4

Salters V J M, Stracke A. 2004. Composition of the depleted mantle. Geochemistry, Geophysics, Geosystems, 5(5): Q05B07, doi: 10.1029/2003GC000597

Schlüter H U, Hinz K, Block M. 1996. Tectono-stratigraphic terranes and detachment faulting of the South China Sea and Sulu Sea. Marine Geology, 130(1–2): 39–78, doi: 10.1016/0025-3227(95)00137-9

Shao Lei, Li Qianyu, Zhu Weilin, et al. 2017. Neogene carbonate platform development in the NW South China Sea: litho-, bio- and chemo-stratigraphic evidence. Marine Geology, 385: 233–243, doi: 10.1016/j.margeo.2017.01.009

Sobolev A V, Hofmann A W, Kuzmin D V, et al. 2007. The amount of recycled crust in sources of mantle-derived melts. Science, 316(5823): 412–417, doi: 10.1126/science.1138113

Sobolev A V, Hofmann A W, Sobolev S V, et al. 2005. An olivine-free mantle source of Hawaiian shield basalts. Nature, 434(7033): 590–597, doi: 10.1038/nature03411

Sobolev S V, Sobolev A V, Kuzmin D V, et al. 2011. Linking mantle plumes, large igneous provinces and environmental catastrophes. Nature, 477(7364): 312–316, doi: 10.1038/nature10385

Sorbadere F, Médard E, Laporte D, et al. 2013. Experimental melting of hydrous peridotite-pyroxenite mixed sources: constraints on the genesis of silica-undersaturated magmas beneath volcanic arcs. Earth and Planetary Science Letters, 384: 42–56, doi: 10.1016/j.epsl.2013.09.026

Sun S S, McDonough W F. 1989. Chemical and isotopic systematics of oceanic basalts: implications for mantle composition and processes. Geological Society, London, Special Publications, 42(1): 313–345, doi: 10.1144/GSL.SP.1989.042.01.19

Sun Liheng, Sun Zhen, Zhang Yunying, et al. 2021. Multi-stage carbonate veins at IODP Site U1504 document Early Cretaceous to early Cenozoic extensional events on the South China Sea margin. Marine Geology, 442: 106656, doi: 10.1016/j.margeo.2021.106656

Suo Yanhui, Li Sanzhong, Jin Chong, et al. 2019. Eastward tectonic migration and transition of the Jurassic-Cretaceous Andean-type continental margin along southeast China. Earth-Science Reviews, 196: 102884, doi: 10.1016/j.earscirev.2019.102884

Thompson R N, Gibson S A. 2000. Transient high temperatures

in mantle plume heads inferred from magnesian olivines in Phanerozoic picrites. Nature, 407(6803): 502–506, doi: 10.1038/35035058

Walter M J. 1998. Melting of garnet peridotite and the origin of komatiite and depleted lithosphere. Journal of Petrology, 39(1): 29–60, doi: 10.1093/petroj/39.1.29

Wan Ling, Yao Bochu, Zeng Weijun, et al. 2006. Lithospheric structure and petroleum distribution in the South China Sea. Geology in China (in Chinese), 33(4): 874–884

Wang Xuance, Li Zhengxiang, Li Xianhua, et al. 2012. Temperature, pressure, and composition of the mantle source region of Late Cenozoic basalts in Hainan Island, SE Asia: a consequence of a young thermal mantle plume close to subduction zones? Journal of Petrology, 53(1): 177–233, doi: 10.1093/petrology/egr061

Wang Xuance, Li Zhengxiang, Li Xianhua, et al. 2013. Identification of an ancient mantle reservoir and young recycled materials in the source region of a young mantle plume: implications for potential linkages between plume and plate tectonics. Earth and Planetary Science Letters, 377–378: 248–259, doi: 10.1016/j.epsl.2013.07.003

Wang Rui, Yu Kefu, Jones B, et al. 2018. Evolution and development of Miocene "island dolostones" on Xisha Islands, South China Sea. Marine Geology, 406: 142–158, doi: 10.1016/j.margeo.2018.09.006

Wei S S, Chen Y J. 2016. Seismic evidence of the Hainan mantle plume by receiver function analysis in southern China. Geophysical Research Letters, 43(17): 8978–8985, doi: 10.1002/2016GL069513

Weller O M, Copley A, Miller W G R, et al. 2019. The relationship between mantle potential temperature and oceanic lithosphere buoyancy. Earth and Planetary Science Letters, 518: 86–99, doi: 10.1016/j.epsl.2019.05.005

Wilkinson J F G, Le Maitre R W. 1987. Upper mantle amphiboles and micas and TiO_2, K_2O, and P_2O_5 abundances and 100 Mg/(Mg+Fe^{2+}) ratios of common basalts and andesites: implications for modal mantle metasomatism and undepleted mantle compositions. Journal of Petrology, 28(1): 37–73, doi: 10.1093/petrology/28.1.37

Wu Shiguo, Yang Zhen, Wang Dawei, et al. 2014. Architecture, development and geological control of the Xisha carbonate platforms, northwestern South China Sea. Marine Geology, 350: 71–83, doi: 10.1016/j.margeo.2013.12.016

Xia Qunke, Bi Yao, Li Pei, et al. 2016a. High water content in primitive continental flood basalts. Scientific Reports, 6: 25416, doi: 10.1038/srep25416

Xia Shaohong, Gou Tao, Zhao Fang, et al. 2025. Late Cenozoic magmatism of the South China Sea driven by the Hainan mantle plume. Science Bulletin, 70(5): 604–608, doi: 10.1016/j.scib.2024.12.010

Xia Qunke, Liu Jia, Liu Shaochen, et al. 2013. High water content in Mesozoic primitive basalts of the North China Craton and implications on the destruction of cratonic mantle lithosphere. Earth and Planetary Science Letters, 361: 85–97, doi: 10.1016/j.epsl.2012.11.024

Xia Shaohong, Zhao Dapeng, Sun Jinlong, et al. 2016b. Teleseismic imaging of the mantle beneath southernmost China: new insights into the Hainan plume. Gondwana Research, 36: 46–56, doi: 10.1016/j.gr.2016.05.003

Xu Yigang, Wei Jingxian, Qiu Huaning, et al. 2012. Opening and evolution of the South China Sea constrained by studies on volcanic rocks: preliminary results and a research design. Chinese Science Bulletin, 57(24): 31503164, doi: 10.1007/s11434-011-4921-1

Yan Quanshu, Castillo P, Shi Xuefa, et al. 2015. Geochemistry and petrogenesis of volcanic rocks from Daimao Seamount (South China Sea) and their tectonic implications. Lithos, 218–219: 117–126, doi: 10.1016/j.lithos.2014.12.023

Yan Pin, Deng Hui, Liu Hailing, et al. 2006. The temporal and spatial distribution of volcanism in the South China Sea region. Journal of Asian Earth Sciences, 27(5): 647–659, doi: 10.1016/j.jseaes.2005.06.005

Yan Quanshu, Shi Xuefa, Castillo P R. 2014. The late Mesozoic-Cenozoic tectonic evolution of the South China Sea: a petrologic perspective. Journal of Asian Earth Sciences, 85: 178–201, doi: 10.1016/j.jseaes.2014.02.005

Yan Quanshu, Shi Xuefa, Metcalfe I, et al. 2018. Hainan mantle plume produced Late Cenozoic basaltic rocks in Thailand, Southeast Asia. Scientific Reports, 8(1): 2640, doi: 10.1038/s41598-018-20712-7

Yan Quanshu, Shi Xuefa, Wang Kunshan, et al. 2008. Major element, trace element, and Sr, Nd and Pb isotope studies of Cenozoic basalts from the South China Sea. Science in China Series D: Earth Sciences, 51(4): 550–566, doi: 10.1007/s11430-008-0026-3

Yan Quanshu, Straub S, Shi Xuefa. 2019. Hafnium isotopic constraints on the origin of late Miocene to Pliocene seamount basalts from the South China Sea and its tectonic implications. Journal of Asian Earth Sciences, 171: 162–168, doi: 10.1016/j.jseaes.2018.06.027

Yang Shuying. 2015. Geochemical characteristics of basalts from the Daimao seamount in the South China Sea (SCS) and from the SCS's neighboring lands: implications for the regional tectonic evolution (in Chinese)[dissertation]. Beijing: China University of Geosciences (Beijing)

Yang Shuying, Fang Nianqiao. 2015. Geochemical variation of volcanic rocks from the South China Sea and neighboring land: implication for magmatic process and mantle structure. Acta Oceanologica Sinica, 34(12): 112–124, doi: 10.1007/s13131-015-0759-8

Yang Fan, Huang Xiaolong, Xu Yigang, et al. 2019. Plume-ridge interaction in the South China Sea: thermometric evidence from Hole U1431E of IODP Expedition 349. Lithos, 324–325: 466–478, doi: 10.1016/j.lithos.2018.11.031

Yang Fan, Huang Xiaolong, Xu Yigang, et al. 2023. Bifurcation of mantle plumes by interaction with stagnant slabs in the mantle transition zone: evidence from late Cenozoic basalts within Southeast Asia. GSA Bulletin, 135(9–10): 2710–2720, doi: 10.1130/B36558.1

Yang Zongfeng, Li Jie, Liang Wenfei, et al. 2016. On the chemical markers of pyroxenite contributions in continental basalts in eastern China: implications for source lithology and the origin of basalts. Earth-Science Reviews, 157: 18–31, doi: 10.1016/j.earscirev.2016.04.001

Yang Wenjian, Yu Hongmei, Zhao Bo, et al. 2020. Mantle

sources and magma genesis of Late Cenozoic basalts in Weizhou Island, Guangxi, China. Acta Petrologica Sinica (in Chinese), 36(7): 2092–2110, doi: 10.18654/1000-0569/2020.07.11

Yao Bochu, Wan Ling, Wu Nengyou. 2004. Cenozoic plate tectonic activities in the Great South China Sea area. Geology in China (in Chinese), 31(2): 113–122

Yu Xun, Liu Zhifei. 2020. Non-mantle-plume process caused the initial spreading of the South China Sea. Scientific Reports, 10(1): 8500, doi: 10.1038/s41598-020-65174-y

Yu Mengming, Yan Yi, Huang Chiyue, et al. 2018. Opening of the South China Sea and upwelling of the Hainan Plume. Geophysical Research Letters, 45(6): 2600–2609, doi: 10.1002/2017GL076872

Zeng Gang, Chen Lihui, Xu Xisheng, et al. 2010. Carbonated mantle sources for Cenozoic intra-plate alkaline basalts in Shandong, North China. Chemical Geology, 273(1–2): 35–45, doi: 10.1016/j.chemgeo.2010.02.009

Zhang Guoliang, Chen Lihui, Jackson M G, et al. 2017. Evolution of carbonated melt to alkali basalt in the South China Sea. Nature Geoscience, 10(3): 229–235, doi: 10.1038/NGEO2877

Zhang Guoliang, Luo Qing, Zhao Jian, et al. 2018a. Geochemical nature of sub-ridge mantle and opening dynamics of the South China Sea. Earth and Planetary Science Letters, 489: 145–155, doi: 10.1016/j.epsl.2018.02.040

Zhang Cuimei, Sun Zhen, Manatschal G, et al. 2021a. Syn-rift magmatic characteristics and evolution at a sediment-rich margin: insights from high-resolution seismic data from the South China Sea. Gondwana Research, 91: 81–96, doi: 10.1016/j.gr.2020.11.012

Zhang Guoliang, Sun Weidong, Seward G. 2018b. Mantle source and magmatic evolution of the dying spreading ridge in the South China Sea. Geochemistry, Geophysics, Geosystems, 19(11): 4385–4399, doi: 10.1029/2018GC007570

Zhang Qiao, Wu Shiguo, Dong Dongdong. 2016. Cenozoic magmatism in the northern continental margin of the South China Sea: evidence from seismic profiles. Marine Geophysical Research, 37(2): 71–94, doi: 10.1007/s11001-016-9266-3

Zhang Qiao, Wu Shiguo, Lv Fuliang, et al. 2014. The seismic characteristics and the distribution of the igneous rocks in the Northernwest slope of the South China Sea. Geotectonica et Metallogenia (in Chinese), 38(4): 919–938

Zhang Yaling, Xu Yigang. 2012. Pyroxenites: high-pressure segregates or recycled oceanic crust? Geological Journal of China Universities (in Chinese), 18(1): 74–87

Zhang Yu, Yu Kefu, Fan Tianlai, et al. 2020a. Geochemistry and petrogenesis of Quaternary basalts from Weizhou Island, northwestern South China Sea: evidence for the Hainan plume. Lithos, 362–363: 105493, doi: 10.1016/j.lithos.2020.105493

Zhang Yu, Yu Kefu, Li Shiying. 2024. U-Pb zircon geochronology of basaltic pyroclastic rocks from the basement beneath the Xisha Islands in the northwestern South China Sea and its geological significance. Acta Oceanologica Sinica, 43(2): 83–93, doi: 10.1007/s13131-023-2198-2

Zhang Yu, Yu Kefu, Qian Handong. 2018c. LA-ICP-MS analysis of clinopyroxenes in basaltic pyroclastic rocks from the Xisha Islands, northwestern South China Sea. Minerals, 8(12): 575, doi: 10.3390/min8120575

Zhang Yu, Yu Kefu, Qian Handong, et al. 2020b. The basement and volcanic activities of the Xisha Islands: evidence from the kilometre-scale drilling in the northwestern South China Sea. Geological Journal, 55(1): 571–583, doi: 10.1002/gj.3416

Zhang Yunying, Yuan Chao, Sun Min, et al. 2021b. Contrasting compositions between phenocrystic and xenocrystic olivines in the Cenozoic basalts from central Mongolia: constraints on source lithology and regional uplift. American Mineralogist, 106(2): 251–264, doi: 10.2138/am-2020-7431

Zong Keqing, Klemd R, Yuan Yu, et al. 2017. The assembly of Rodinia: the correlation of early Neoproterozoic (ca. 900 Ma) high-grade metamorphism and continental arc formation in the southern Beishan Orogen, southern Central Asian Orogenic Belt (CAOB). Precambrian Research, 290: 32–48, doi: 10.1016/j.precamres.2016.12.010

Zou Haibo, Fan Qicheng. 2010. U-Th isotopes in Hainan basalts: implications for sub-asthenospheric origin of EM2 mantle endmember and the dynamics of melting beneath Hainan Island. Lithos, 116(1–2): 145–152, doi: 10.1016/j.lithos.2010.01.010

Zou Haibo, Reid M R, Liu Yongshun, et al. 2003. Constraints on the origin of historic potassic basalts from Northeast China by U-Th disequilibrium data. Chemical Geology, 200(1–2): 189–201, doi: 10.1016/S0009-2541(03)00188-8

Supplementary information:

Table S1. Major and trace element compositions of the basaltic pyroclastic rocks from Well CK-2, Xisha Islands, SCS.

Table S2. The chemical compositions of olivines of the basaltic pyroclastic rocks from Well CK-2, Xisha Islands, SCS.

The supplementary information is available online at https://doi.org/10.1007/s13131-025-2511-3 and http://www.aosocean.com/. The supplementary information is published as submitted, without typesetting or editing. The responsibility for scientific accuracy and content remains entirely with the authors.